BB

GSI

GSI-95-33
PREPRINT
JULY 1995

NUCLEON DISTRIBUTIONS OF ^{6}He AND ^{8}He FROM INTERMEDIATE-ENERGY PROTON ELASTIC SCATTERING IN INVERSE KINEMATICS

S.R. NEUMAIER, G.D. ALKHAZOV, M.N. ANDRONENKO, T. BEHA, K.-H. BEHR, A. BRÜNLE, K. BURKHARD, A.V. DOBROVOLSKY, P. EGELHOF, C. FISCHER, G.E. GAVRILOV, H. GEISSEL, H.M. HOFMANN, H. IRNICH, A.V. KHANZADEEV, G.A. KROLEV, A.A. LOBODENKO, P. LORENZEN, G. MÜNZENBERG, M. MUTTERER, F. NICKEL, W. SCHWAB, D.M. SELIVERSTOV, P. SINGER, T. SUZUKI, J.P. THEOBALD (†), N.A. TIMOFEEV, A.A. VOROBYOV, J. WURZER, V.I. YATSOURA

(Proc. of the 'Int. Conf. on Exotic Nuclei and Atomic Masses, ENAM', Arles, France, June 19-23, 1995)

Gesellschaft für Schwerionenforschung mbH
Postfach 110552 · D-64220 Darmstadt · Germany

NUCLEON DISTRIBUTIONS OF ^{6}He AND ^{8}He FROM INTERMEDIATE-ENERGY PROTON ELASTIC SCATTERING IN INVERSE KINEMATICS*)

S.R. Neumaier[1)], G.D. Alkhazov[2)], M.N. Andronenko[2)], T. Beha[3)], K-H. Behr[3)], A. Brünle[3)], K. Burkhard[3)], A.V. Dobrovolsky[2)], P. Egelhof[3)], C. Fischer[3)], G.E. Gavrilov[2)], H. Geissel[3)], H. M. Hofmann[4)], H. Irnich[3)], A.V. Khanzadeev[2)], G.A. Korolev[2)], A.A. Lobodenko[2)], P. Lorenzen[1)], G. Münzenberg[3)], M. Mutterer[1)], F. Nickel[3)], W. Schwab[3)], D.M. Seliverstov[2)], P. Singer[1)], T. Suzuki[3)], J.P. Theobald[1)] (†), N.A. Timofeev[2)], A.A. Vorobyov[2)], J. Wurzer[4)], V.I. Yatsoura[2)]

[1)]Institut für Kernphysik, Technische Hochschule, 64289 Darmstadt, Germany
[2)]Petersburg Nuclear Physics Institute, 188350 Gatchina, Russia
[3)]Gesellschaft für Schwerionenforschung, 64220 Darmstadt, Germany
[4)]Institut für Theoretische Physik, Universität Erlangen, 91058 Erlangen, Germany

ABSTRACT

Nuclear matter density distributions of ^{4}He and the neutron-rich nuclei ^{6}He and ^{8}He were studied via intermediate-energy proton nucleus scattering in inverse kinematics using the recoil detector IKAR. For these nuclei, differential cross sections for elastic scattering at low momentum transfer were measured with an accuracy of 2% on absolute normalization. The experimental method and the procedure of data analysis are described. Phenomenological and microscopically calculated nuclear matter distributions were related to the measured cross sections with the aid of the Glauber multiple scattering theory.

1. INTRODUCTION

The use of protons with energies of 700 - 1000 MeV as probes has proved to be a well suited method to study nuclear matter density distributions of stable nuclei. At intermediate energies, elastic proton-nucleus scattering can be described with good accuracy by diffractive multiple scattering theory which is able to relate measured differential cross sections to the nuclear matter radii of interest in a rather unambiguous way[1]. This method can also be applied to study unstable nuclei by measuring proton elastic scattering in inverse kinematics using radioactive beams. Furthermore, theoretical

estimates[2] have indicated that proton scattering in the region of low momentum transfer $|t| < 0.05$ GeV^2/c^2 may be sensitive to probe matter distributions that have extended neutron tails, characteristic for light neutron-rich nuclei near or at the neutron drip line[3]. This new type of nuclear structure with unusually large nuclear rms-radii has been explored by measurements of total interaction and reaction cross sections[4], and investigated further by measuring momentum distributions of the reaction products[5,6]. In the present work, intermediate-energy radioactive beams available at GSI Darmstadt were applied to measure, in inverse kinematics, differential cross sections for proton elastic scattering on helium nuclei.

2. GLAUBER MULTIPLE SCATTERING THEORY

To deduce information on the nuclear matter density distributions from measured cross sections the Glauber multiple scattering theory can be applied. The cross section $d\sigma/dt$ is given by

$$\frac{d\sigma}{dt} = \frac{d\sigma}{d\Omega}\frac{\pi}{p^2} = \left|F(q)^2\right|\frac{\pi}{p^2} \qquad (1)$$

The Mandelstamm variable $-t$ is defined as the negative square of the four-momentum transfer q, and p is the momentum of the projectile. The scattering amplitude $F(q)$ is given by

$$F(q) = -2\zeta\,\frac{k}{q^2}\,e^{i\varphi_c} + f_1(q) \qquad (2)$$

$$f_1(q) = \frac{ik}{2\pi}\int J_0(qb)\,db\left\{e^{i\chi_0(b)} - \left[1-\gamma_p(b)\right]^Z\left[1-\gamma_N(b)\right]^N\; e^{i\chi_p(b)}\right\} \qquad (3)$$

Quantities Z and N are the nuclear charge and the neutron number, respectively. The first term in eq. 2 and the exponentials in eq. 3 describe the Coulomb part of $F(q)$[7]. The profile functions γ_P, γ_N are evaluated by a Fourier transformation of the elementary nucleon-nucleon scattering amplitudes $f_j(q)$ and the form factors $S(q)$ of the one-body-density distributions involved. $J_0(x)$ is the Bessel-function of 0th order, and b represents the impact parameter.

$$\gamma_j(b) = \frac{1}{ik}\int_0^\infty J_0(q'b)\,f_j(q')\,S(q')q'\,dq' \qquad (4)$$

$$f_j^c(q) = \frac{k\,\sigma_j}{4\pi}\left(\varepsilon_j + i\right) e^{-\frac{q^2\beta_j^2}{2}} \quad \text{with } j = [pp,pn] \qquad \textbf{(5)}$$

Only the scalar parts of the elementary proton-proton (*pp*) and proton-neutron (*pn*) scattering amplitudes are used. These are parametrized by complex Gaussians, with σ_j, ε_j and β_j, being the total cross sections, the ratios of the real-to-imaginary part and the slope parameters, respectively. The energy dependence of the parameters was taken into account by interpolating experimental values obtained from phase-shift analysis[8].

To extract information on the nuclear matter distribution of the helium isotopes we have performed calculations with introducing phenomenological one-body-density distributions of Gaussian and Fermi type and determine their rms-radii by fitting the measured cross sections by the method of least squares. Furthermore, differential cross sections resulting from density distributions as determined from microscopic calculations according to the Refined Resonating Group Model (RRGM)[9] were compared with the data.

3. EXPERIMENTAL METHOD

The experiment was performed at the heavy-ion synchrotron (SIS) of GSI Darmstadt. ^{18}O projectiles were extracted from SIS at 820 MeV/u and 730 MeV/u and focused on an 8 g/cm^2 beryllium target at the entrance of the fragment separator FRS[10]. The higher projectile energy was used for the production of ^4He and ^6He secondary beams, whereas the lower one was used for ^8He. The two lighter He beams were separated in the FRS with magnetic-rigidity analysis in combination with atomic energy loss in an achromatic 20 g/cm^2 aluminum degrader placed at the dispersive central focal plane. Although the thickness of the degrader in terms of the range of the He beams is only 0.05, the separation power was sufficient to reduce the background to an order of 1%. Discrimination from beam contaminants that have other nuclear charges than He is attained by an energy-loss (ΔE) measurement in the experimental setup used. In the present work, projectile energies were chosen to be 699 MeV/u, 717 MeV/u and 674 MeV/u, for ^4He, ^6He and ^8He, respectively.

The setup of detectors (see Fig. 1) to measure elastic proton scattering in inverse kinematics with these projectiles was installed at the final focal plane of the fragment separator. Particle beams with intensities between 10^3 and 10^4 particles per spill are

interacting with protons inside a high-pressure hydrogen filled ionization chamber IKAR[11] which serves simultaneously as a gas target and a recoil-proton detector.

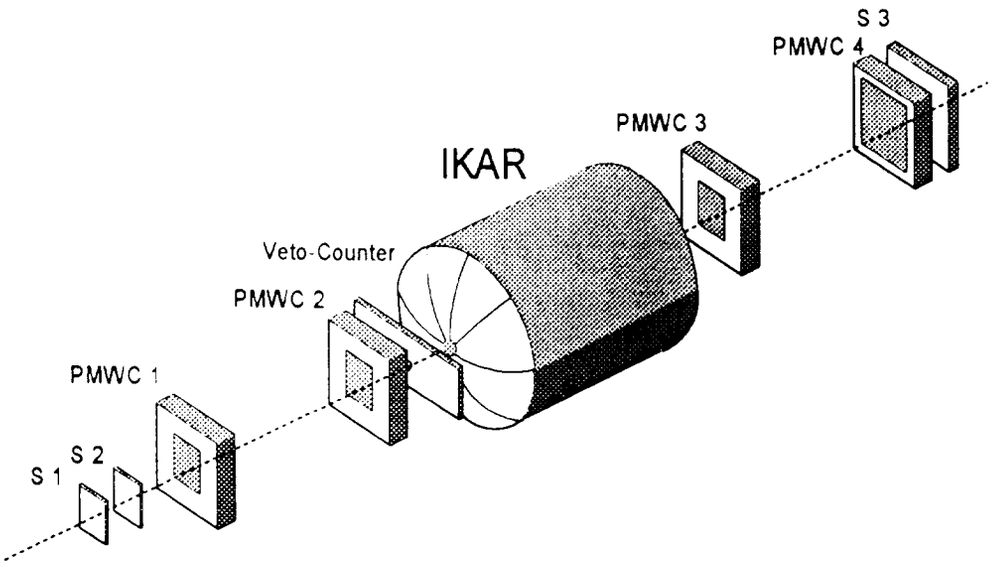

Fig. 1. Schematic view of the experimental setup. The central part shows the hydrogen filled ionization chamber IKAR which serves simultaneously as a gas target and detector system for recoil protons. Four proportional multiwire chambers (PMWC 1- 4) determine the scattering angle of the projectile. A series of scintillation counters (S1 - S3) was used for trigger and particle identification.

This device which was developed at the Petersburg Nuclear Physics Institute (PNPI), Gatchina consists of 6 Frisch-gridded ionization chambers in line, operated with high-purity hydrogen gas at a pressure of 10 bar. Projectile entrance and exit windows of IKAR are semi-spherical shells made of beryllium with a thickness of 0.5 mm. Four two-dimensional position sensitive multi-wire chambers PMWC positioned up and down stream of the IKAR chamber served as tracking detectors for projectile nuclei . A special front-end analog processor unit was used to calculate event-wise the projectile scattering angle from the fast PMWC signals in order to exclude events from registration which pass IKAR with scattering angles of less than 0.2 mrad. A series of thin plastic scintillators (S_1,S_2, and Veto) were used to provide a fast event trigger and to select projectiles that enter IKAR within an area of 2 cm in diameter along its central axis. A thick scintillator (S_3) located at the end of the setup provides the ΔE information for particle identification.

One of the 6 detector cells of IKAR is shown schematically in Fig. 2, along with an illustration of a typical scattering event between a projectile nucleus and a proton from the chamber gas. The active volume in each cell is the space of 10 cm depth between Frisch-grid and cathode. Recoil protons, scattered here essentially in parallel to the electrodes,

are registered with their full energy when their tracks are shorter than the outer radius of 20 cm of the anode plates. This corresponds to a proton energy of 5.2 MeV. Anodes and cathodes of IKAR are stainless-steel discs with their central parts replaced by aluminum foils of 5 mg/cm^2 thickness to minimize the material along the path of the projectiles. Each anode plate is further subdivided into an inner part (Anode A) of 10 cm radius which is a double electrode in order to register signals from adjacent cells separately, and an outer part (Anode B) which registers signals from neighboring cells simultaneously. This structure of electrodes was chosen in order to provide a minimum number of data channels necessary to identify unambiguously in which chamber cell a measured scattering event had occurred. Minimization of material is also important to maintain the high purity of 99.9999 % of the hydrogen gas throughout a few weeks of experiment. Chamber performance and gas purity is monitored with the aid of pulses from various ^{241}Am α sources evaporated onto each cathode plate and onto part of the Frisch-grids.

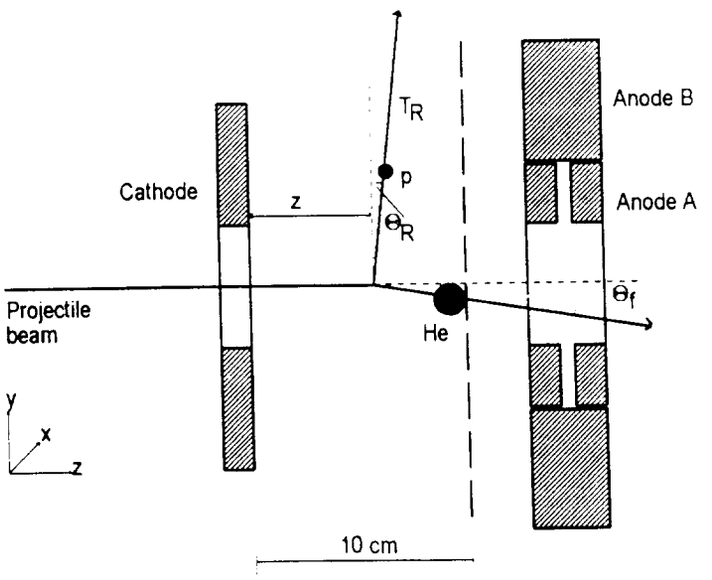

Fig. 2. Schematic view of one of the six ionization chamber modules in IKAR. Measured figures are the proton recoil energy T_R, the recoil angle Θ_R, and the distance Z of the vertex point from the cathode.

4. DATA ANALYSIS AND NORMALIZATION PROCEDURES

For each scattering event, signals from anodes A and B and from the cathode of a detector cell concerned were registered by 8-bit flash-type ADCs, with a time period of 25 μs. This techniques allows to determine in the off-line analysis various parameters of an individual proton signal. The integral over induced charges precisely determines (with a resolution ΔT_R^* of 70 keV) the energy T_R^* of the recoil protons, or their energy loss in case their ranges exceed the active chamber volume. From the location of a proton pulse in the flash-ADC spectrum and from its characteristic shape, the interaction vertex in the

grid-cathode space can be reconstructed, as well as the projection of the track of the recoil proton on the beam axis. These data were used, together with the position information on projectile angles delivered by the tracking detectors, to reconstruct the kinematic relation for elastic scattering between the projectile scattering angle Θ_F and the energy T_R of the recoil protons.

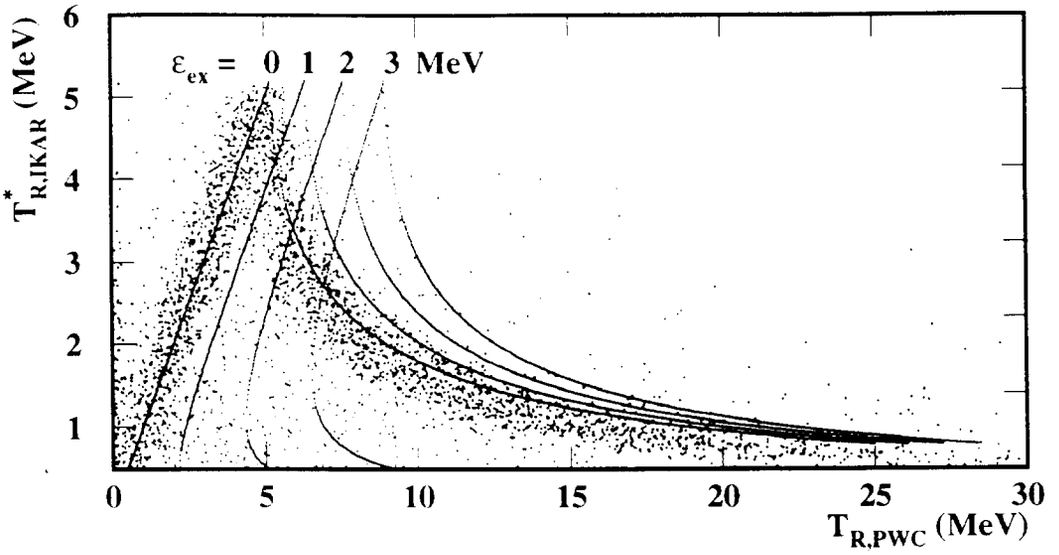

Fig. 3. Proton energy T_R^* deposited in IKAR, versus proton energy T_R calculated from measured ^{8}He projectile angles Θ_F assuming elastic scattering. Calculated curves that simulate excited states of 1, 2 and 3 MeV are plotted to illustrate the kinematical separation of non-elastic events.

Figure 3 depicts the correlation of the fraction T_R^* of the proton energy deposited in IKAR with proton energy T_R as calculated from the measured projectile angles Θ_F assuming elastic scattering. Calculated curves that simulate elastically scattered events, and events that would lead to projectile excited states at 1, 2, and 3 MeV are also shown. By the correlation shown in Fig. 3, possible contributions from inelastic scattering into states of more than 1 MeV excitation energy can be excluded. This holds also for the 2n break-up channels in ^{6}He and ^{8}He, with 2n separation energies of 0.97 MeV and 2,13 MeV, respectively. Figure 3 shows also, that background events outside the elastic curve are randomly distributed and rather scarce (typically below 3% for each energy bin) and can be corrected straightforward.

An important issue is the absolute normalization procedure of the differential cross section measured. This is done with the knowledge on the integral number M of projectiles registered and the effective number of target nuclei N_T . The number M was monitored continuously during the experiment by processing signals from the various scintillators,

considering the influence of dead times during data acquisition, beam impurities ect.. The residual bond of systematic errors on the final value of the integral monitor number is estimated to be 2%. The effective thickness of the target was determined with an accuracy of better than 0.2% by precise registration of gas pressure and temperature during the runs, and from the effective depths of the six active chamber volumes. The latter were considered dependent on the recoil energy because of the variation of the proton recoil angle Θ_R with T_R.

5. EXPERIMENTAL RESULTS

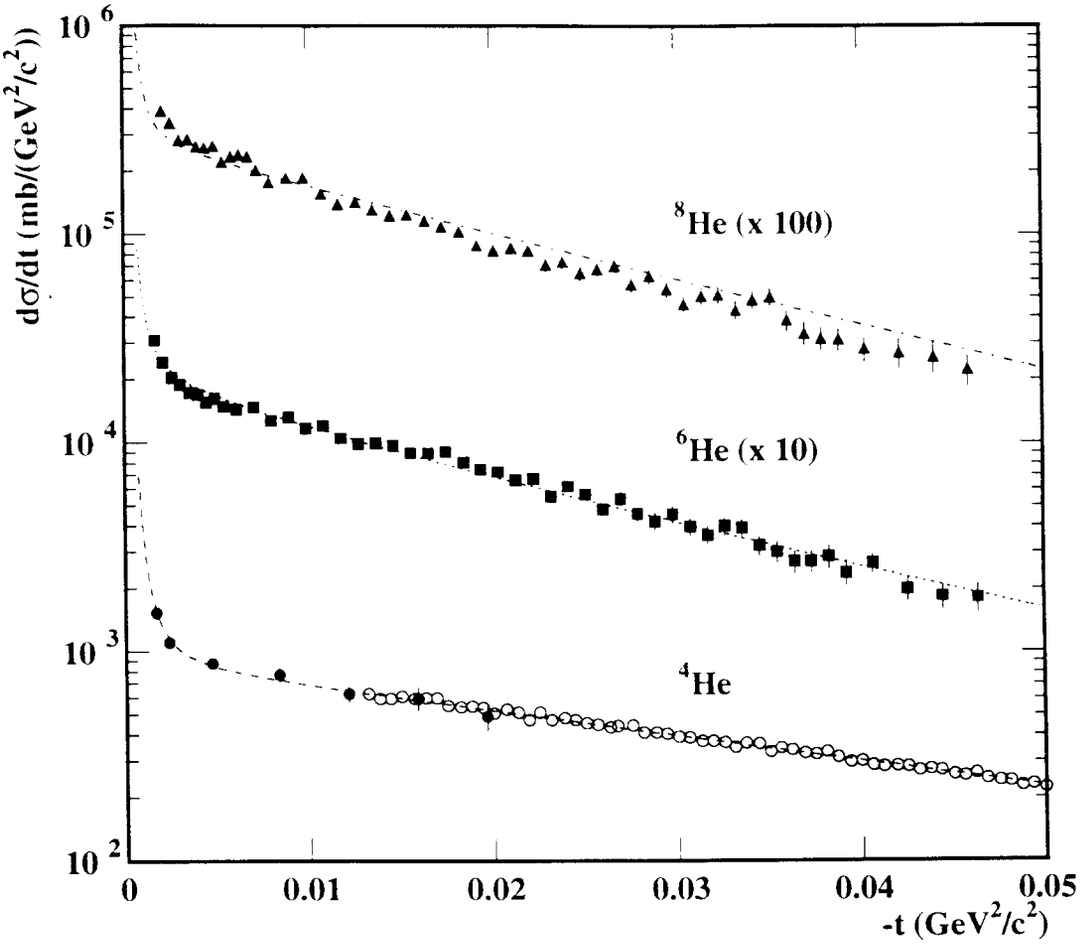

Fig. 4. Absolute differential cross section $d\sigma/dt$ versus the four momentum transfer squared $|t|$ for p^4He, p^6He and p^8He elastic scattering measured in the present experiment (full symbols). Open dots show the result of an earlier measurement of p^4He scattering which was performed in direct kinematics with a proton beam[12]. Dashed lines are calculated curves resulting from nuclear matter distributions as postulated by the RRGM theory (SZ-V2, see chapt. 6).

The experimental results on the cross sections are shown in Fig. 4. The plotted error bars consider statistical errors only. Total numbers of events in these spectra are $3 \cdot 10^4$ for ^6He and ^8He each, and $5 \cdot 10^3$ for ^4He. In the case of ^4He (full dots) an excellent

overall agreement with data by Grebenjuk et al.[12] is attained. These data (open dots) were obtained, with better statistical accuracy, in direct kinematics using a proton beam and the IKAR chamber operated with helium as counting gas. The favorable situation of higher energies of recoil particles in the case of inverse kinematics has allowed to supplement these experimental data for the region of low momentum transfer.

6. DEDUCTION OF NUCLEAR MATTER DISTRIBUTIONS

To describe the p^{4}He cross-section, Gaussian and Fermi one-body density distributions folded with the finite size of the nucleons[a] ($r_{rms} = \langle r^2 \rangle^{1/2} = 0.8$ fm) were fitted to the present data and those from Ref[12]. Alternatively, a parametrization by a sum of 12 Gaussians used to describe the nuclear charge distribution[13] was taken as the nuclear matter distribution to calculate the differential cross section. Measured data can be well reproduced with all of these approaches giving a reduced χ^2 around unity. The folded matter rms-radius obtained by the fits is 1.67 ± 0.05 fm which corresponds to a point matter radius of 1.45 ± 0.05 fm. This value agrees with 1.45 fm as measured for the distribution of nuclear charge. A ^{4}He point matter density distribution calculated in the frame of the RRGM theory and using an effective nucleon-nucleon force introduced by Stöwe and Zahn[9] yields $r_{rms} = 1.42$ fm. Results of this calculations describe the measured cross section also with good accuracy (see Fig. 4).

For ^{6}He scattering, a best fit was obtained using a point matter density parametrized by one Gaussian for the proton distribution and a composition of two Gaussians for the neutrons. One of these is assumed to contain 2 neutrons and to have the same radius as the proton distribution, and the second one approximating the distribution of two valence neutrons. Fit results are listed in table 1, with an average $r_{rms} = 2.35 \pm 0.09$ fm. An assumption of a nuclear density distribution with the same rms-radius for a single Gaussian containing all 6 nucleons fails to describe the cross section. From the RRGM theory, the density distributions (see Fig. 5 left side) with the Stöwe and Zahn force again give the best description of the data. The original version[9], abbreviated SZ-2 in table 1, omits the central force terms in the odd parity singlet and triplet states of the nucleon-nucleon two-body force, whereas version SZ-V2 includes all terms. The repulsive force of these terms increases the phase space, which leads to a slightly larger

---

[a]The folded matter distribution is used to be comparable to the nuclear charge distribution which is available as a folded density distribution

rms-radius. From these microscopic calculations one gets a hint about the effective size of the α-like core in ^{6}He. The larger proton radius in ^{6}He can be explained by a ^{4}He-core with a size comparable to the free α particle but increased by an overlapping center-of-mass motion.

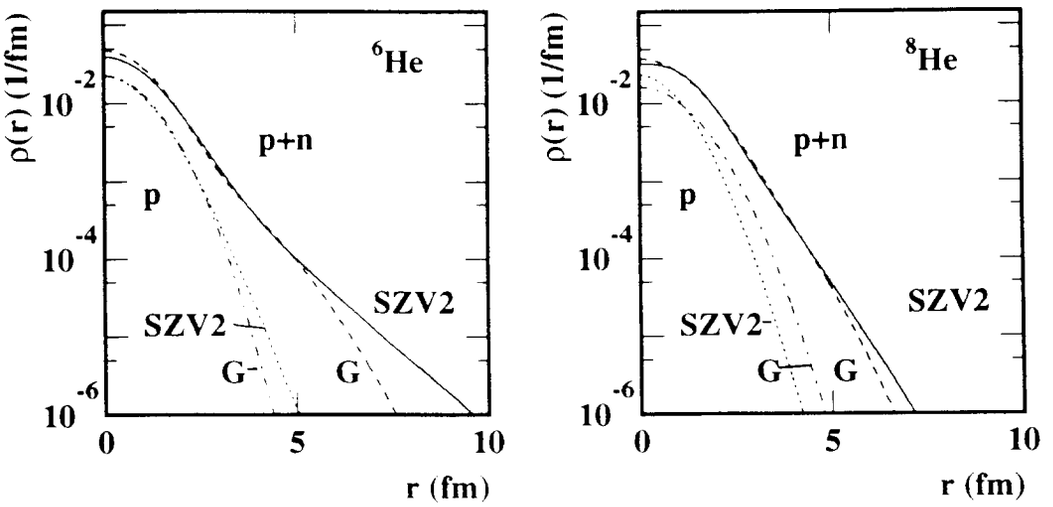

Fig. 5. Proton and nuclear matter distributions of ^{6}He (left side) and ^{8}He (right side) calculated in the frame of the RRGM theory including the central force terms in all two-body nucleon-nucleon forces (SZ-V2, dotted and full lines), compared with the results from the two-Gaussian fits (dashed-dotted and dashed lines).

isotope	distribution	R_p (fm)	R_n (fm)	R_m (fm)
^{4}He	one-Gaussian (fit)	1.45 ± 0.05	1.45 ± 0.05	1.45 ± 0.05
^{4}He	RRGM (SZ-V2)	1.42	1.42	1.42
^{6}He	two-Gaussian (fit)	1.70 ± 0.07	2.62 ± 0.12	2.35 ± 0.09
^{6}He	RRGM (SZ-2)	1.75	2.59	2.34
^{6}He	RRGM (SZ-V2)	1.79	2.77	2.49
^{8}He	two-Gaussian (fit)	1.89 ± 0.17	2.50 ± 0.19	2.37 ± 0.18
^{8}He	RRGM (SZ-2)	1.54	2.21	2.06
^{8}He	RRGM (SZ-V2)	1.56	2.30	2.14

Table 1. Root mean square radii of the proton, neutron and nuclear point matter distributions for the ^{6}He and ^{8}He isotope. (for explanations see text)

In the case of ^{8}He we have deduced the radii of proton and neutron distributions the same way, but assuming 4 valence neutrons instead of 2. The best fit is again obtained by a two-Gaussian neutron distribution, but fitting a single Gaussian gives only a

slightly worse description of the data. Taking into account the knowledge about the sensitivity of elastic proton scattering for $|t| < 0.05$ GeV^2/c^2 to the shape of the density distribution, there is reason to believe that proton and neutron radii in ^{8}He are not as different as in ^{6}He (see Fig. 5).

At present, calculations in the framework of the RRGM theory for the ^{8}He nucleus are not yet converged (due to problems concerning the required computing time), but nevertheless all neutron density distributions calculated reveal a less pronounced tail for ^{8}He, too. Note, that the discussion concerning the tail deals with contributions to the density in the order of magnitude $\rho(r) < 10^{-3}$ fm^{-1}.

7. SUMMARY

Intermediate-energy proton elastic scattering on exotic nuclei in inverse kinematics has been shown to be a powerful tool to provide information on nuclear density distributions. The proton recoil detector IKAR is well suited to perform such measurements. The differential cross section is observed to reflect the extensions of neutron matter distributions. In the present work the accuracy on the deduced nuclear density parameters is mainly due to the limitation in counting statistics. Measurements with radioactive beams of neutron-rich lithium and beryllium isotopes using the same experimental techniques are in preparation.

---

*) This work forms part of the PhD Thesis of S. R. Neumaier, and was supported by BMFT (06DA461) and the Sci.& Techn. Coop. Progr. between Germany and Russia. One of us (J. W.) wants to acknowledge support by DFG and BMBF.

REFERENCES

[1] G. D. Alkhazov et al., Phys. Rep. C,Vol. 42 (1978) 89
[2] G. D. Alkhazov and A.A. Lobodenko, Proc. Int. Conf. on Nuclei far from Stability, Bernkastel-Kues, Germany, (1992), IOP-Publishing, p. 341
[3] P.G. Hansen, Nucl. Phys A 553 (1993) 89c
[4] I. Tanihata et al., Phys. Lett. B 289 (1992) 261
[5] F. Humbert et al., Phys. Lett. B 347 (1995) 198
[6] T. Nilsson et al. Europhys. Lett. 30 (1995) 19
[7] R. J. Glauber, Proc. of the 3. Int. Conf. on high energy physics and nuclear structure, New York (1970)
[8] J.A. McNeil et al., Phys. Rev. C Vol. 27 (1983) 2123
[9] T. Mertelmeier and H.M. Hofmann, Nucl. Phys. A 459 (1986) 387
[10] H. Geissel et al., Nucl. Instr. and. Meth. B70 (1992) 286
[11] A. A. Vorobyov et al., Nucl. Instr. and Meth. 119 (1974) 509
[12] O. G. Grebenjuk et al., Nucl. Phys. A 500 (1989) 637
[13] H. Devries et al. Atomic Data and Nuclear Data Tables 36 (1987) 495-536